

# Droplet generation in micro-sieve dispersion device

K. Wang · Y. C. Lu · J. H. Xu · G. S. Luo

Received: 15 September 2010 / Accepted: 1 November 2010 / Published online: 23 November 2010  
© Springer-Verlag 2010

**Abstract** Microfluidic devices with micro-sieve plate as the dispersion medium have been widely used for the mass production of emulsions. While unfortunately, few studies have so far been made for the droplet generation rules in those devices. In this work, the droplet generation processes in micro-sieve dispersion devices are investigated with specially designed micro-sieve pore arrays. The effects of channel structure, pore arrangement, and feeding method of dispersed phase on the average size and distribution of droplets are studied carefully. It is found the dimensionless average droplet diameters ( $d_{av}/d_c$ ) in micro-sieve dispersion devices can be represented by a linear relation with  $Ca^{-1/4}$  of continuous phase, the same as the scaling law in T-junction microchannels. The flow distribution among pores and the steric hindrance between droplets affect the diameter distribution of generated droplet very much. Monodispersed droplets with polydispersity index less than 5% can be made at Ca number larger than 0.01 and phase ratio ( $Q_D/Q_C$ ) less than 1/6 in the present investigation.

**Keywords** Micro-sieve dispersion · Microfluidic device · Droplet generation · Emulsion

## 1 Introduction

The design of new and improved emulsification techniques is very important for the development of chemical, medical, biological, and food industries. During recent years, the growing trend in microfluidic device facilitates reducing the dispersion scale of emulsions into microscale (Engl et al. 2008; Teh et al. 2008). Monodispersed microbubbles and microdroplets can be controllably prepared in microfluidic devices (Choi et al. 2010; Marmottant and Raven 2009) and it has been proved that the microdispersed emulsion systems have good transport and reacting properties (Panic et al. 2004; Xu et al. 2008a). Using these properties, microfluidic devices can be applied to enhance chemical reactions (Razzaq et al. 2009), prepare microsphere materials (Park et al. 2009), synthesize nanoparticles (Sevonkaev and Matijevic 2009), provide biological analysis (Felbel et al. 2008), develop fuel cells (Kjeang et al. 2009), and so on. For the purpose of giving accurate control of the emulsification process, the basic studies on droplet/bubble generation rules in microfluidic devices are very important.

During recent years, researchers have made a lot of investigations on the generation rules of droplet/bubble in T-junction (Xu et al. 2008b), flow-focusing (Nie et al. 2008), co-pipes (Guillot et al. 2007), and some other microfluidic devices (Lao et al. 2009). Based on the methods of experimental research (van Steijn et al. 2009), theory analysis (Steggmans et al. 2009), and computational simulation (de Menech et al. 2008), the break-up mechanisms of droplets and bubbles have been revealed adequately. It is found that the droplet/bubble generation process is mainly dominated by the shearing force and interfacial tension (Christopher et al. 2008). The capillary number of continuous phase ( $Ca_C = \mu_C u_C / \gamma$ ) is a key

K. Wang (✉) · Y. C. Lu · J. H. Xu · G. S. Luo (✉)  
The State Key Lab of Chemical Engineering, Department  
of Chemical Engineering, Tsinghua University,  
Beijing 100084, China  
e-mail: kaiwang@tsinghua.edu.cn

G. S. Luo  
e-mail: gsluo@tsinghua.edu.cn

parameter affecting the flow pattern (Cubaud and Mason 2008) and the droplet size (Xu et al. 2006).

Microchannels are effective tools for the investigation of single droplet generation. However, the running capacity of a single microchannel is very low. For the engineering applications of emulsion, the mass production of microdroplets or microbubbles is strongly called for. Several methods have been designed to give a mass production of emulsions, such as spontaneous emulsification with microchannel array (Kobayashi et al. 2008), shear-induced emulsification with micro-junction array (Nisisako and Torii 2008), and shear-induced emulsification with micro-sieve plate (Geerken et al. 2008). Among those methods, the cross flow shearing micro-sieve dispersion devices are usually used (Gijbetsen-Abrahamse et al. 2004). Abrahamse et al. (2002) gave an investigation on the droplet generation process with a micro-sieve device and they found the droplet diameter decreased with an increasing number of active pores. Geerken et al. (2007) found the droplet size changes little with the variation of the trans-pressure through the micro-sieve pores. In our previous works, two micro-sieve dispersion devices with  $3 \times 3$  and  $4 \times 4$  pore arrays were made to prepare nano particles (Li et al. 2009a). It was found that the droplets were generated regularly in both devices.

Previous works above are important for understanding the droplet generation rules in micro-sieve dispersion device. However, comparing with the adequate researches in common T-junction microfluidic devices, which have a

similar structure to micro-sieve dispersion devices, discussions about the droplet generation rules in multi-pore dispersion processes are not enough, especially for the droplet scaling law and the size distribution control. Our previous work gave such an investigation in the simplest micro-sieve dispersion device—double-pore dispersion device, and it was found that uniform droplets ruptured alternately above the micro-sieve pore array (Wang et al. 2009a). In this work, we try to give a further study in this area using 11 microfluidic devices with specially designed pore arrays. The effects of channel structure, pore arrangement, and feeding method of dispersed phase on the average size and distribution of droplets are carefully examined. Comparisons between micro-sieve dispersion process and single-pore dispersion process are also made to give a clear display of the droplet generation rules.

## 2 Experimental

### 2.1 Micro-sieve dispersion devices

The micro-sieve dispersion devices were fabricated on polymethyl methacrylate (PMMA) chips with end mills. After fabrication, the chips were sealed with supersonic-assisted sealing technique (Li et al. 2009b) and then connected to Teflon pipes. The main structures of those devices are shown in Fig. 1. The main channels shown with solid lines are used to generate droplets and the wide

**Fig. 1** The schematic diagrams of micro-sieve dispersion devices in the experiment.  $D_1$ – $D_{11}$  are their labels. The black lines show the channel walls and the pores on the top layer. The dash lines represent the inlet channels and inlet chambers of dispersed phase on the bottom layer. The flow directions are shown with solid arrows. Some supplied words are pointed out with open arrows

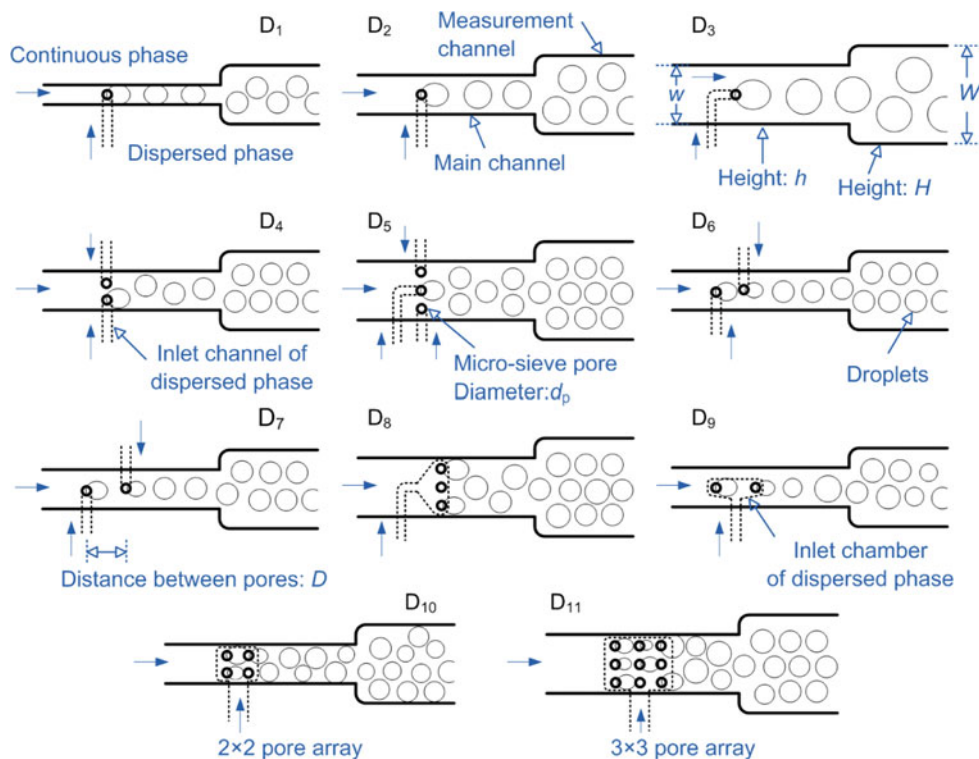


**Table 1** The structural parameters of the micro-sieve dispersion devices

| Devices         | $w$ (mm) | $h$ (mm) | $W$ (mm) | $H$ (mm) | $d_p$ (mm) | $D$ (mm)                            |
|-----------------|----------|----------|----------|----------|------------|-------------------------------------|
| D <sub>1</sub>  | 0.6      | 0.6      | 2.0      | 0.8      | 0.3        | –                                   |
| D <sub>2</sub>  | 1.2      | 0.6      | 2.5      | 0.8      | 0.3        | –                                   |
| D <sub>3</sub>  | 1.8      | 0.6      | 3.0      | 0.8      | 0.3        | –                                   |
| D <sub>4</sub>  | 1.2      | 0.6      | 2.5      | 0.8      | 0.3        | 0.6                                 |
| D <sub>5</sub>  | 1.8      | 0.6      | 3.0      | 0.8      | 0.3        | 0.6                                 |
| D <sub>6</sub>  | 1.2      | 0.6      | 2.5      | 0.8      | 0.3        | 1.0                                 |
| D <sub>7</sub>  | 1.2      | 0.6      | 2.5      | 0.8      | 0.3        | 2.0                                 |
| D <sub>8</sub>  | 1.8      | 0.6      | 3.0      | 0.8      | 0.3        | 0.6                                 |
| D <sub>9</sub>  | 1.2      | 0.6      | 2.5      | 0.8      | 0.3        | 2.0                                 |
| D <sub>10</sub> | 1.2      | 0.6      | 2.5      | 0.8      | 0.3        | 0.6 <sup>r</sup> ; 1.2 <sup>a</sup> |
| D <sub>11</sub> | 1.8      | 0.6      | 3.0      | 0.8      | 0.3        | 0.6 <sup>r</sup> ; 1.2 <sup>a</sup> |

<sup>r</sup> Refers to the radial direction and <sup>a</sup> refers to the axial direction

channels are made for observation and recording pictures. The micro-sieve pores are placed on the bottom of the main channel. These microfluidic devices have two layers, as shown in Fig. 1. The main channel and the measurement channel are made in the top layer. The inlet channel and inlet chamber of dispersed phase drawn with dash lines are placed as the bottom layer. These two layers are connected by the micro-sieve pores only. In order to give a clear display of the droplet generation process, the numbers of the micro-sieve pores are designed not more than 3 in microdevices D<sub>1</sub>–D<sub>9</sub>. The widths of the main channel are varied from 0.6 to 1.8 mm in the experiment. For the layout of micro-sieve pores, three kinds of arrangements, *single pore* (D<sub>1</sub>, D<sub>2</sub>, and D<sub>3</sub>), *radial-array pore* (D<sub>4</sub>, D<sub>5</sub>, and D<sub>8</sub>), and *axial-array pore* (D<sub>6</sub>, D<sub>7</sub>, and D<sub>9</sub>) are chosen. For the feeding of dispersed phase, two methods are adopted: *independent-pore* dispersion, which refers to the micro-sieve pores that have independent inlet channels with independent feeding systems (D<sub>4</sub>, D<sub>5</sub>, D<sub>6</sub>, and D<sub>7</sub>), and *connected-pore* dispersion, which refers to the micro-sieve pores connected by one inlet chamber (D<sub>8</sub>, D<sub>9</sub>). The dispersed phase fluids have equal flow rates passing through the pores in the independent-pore devices and have equal incoming pressures in the inlet chambers of the connected-pore devices. In the end, two commonly used micro-sieve dispersion devices with 2 × 2 and 3 × 3 pore arrays (D<sub>10</sub>, D<sub>11</sub>) are developed to test the obtained generation rules. The structure parameters of those microfluidic devices are given in Table 1.

## 2.2 Operation and analysis

The working system in the experiment was *n*-heptane/3wt% SDS solution (sodium dodecyl sulfate aqueous solution). The experiment was made at 25°C and the

physical properties of the working system were measured with an Ubbelohde viscometer and a pendant drop interfacial tension meter (OCAH200, DataPhysics Instruments GmbH, Germany) at that temperature. The viscosity of the SDS solution is 1.05 mPa s. The interfacial tension is 4.82 mN/m. All flow rates were controlled by syringe pumps (TS-1B, Longer, China) with gastight syringes. Considering the effect of surfactant on the wetting property of channel walls, the continuous phase was pumped into the experimental devices 2 h before the dispersed phase was added in. Different flow rates of working system were tested in the experiment. After changing any of the operating parameter, it was allowed at least 1 min of equilibration time. Since high concentration of ionic surfactant was used in the continuous phase, no droplet coalescence occurred in the present experiment.

Experiments were carried out with a microscope that had a high-speed CCD video camera (PL-A742, PixeLINK, Canada). Images and videos were recorded at a constant frequency (200 Hz). The size of the oil droplet was characterized by the volumetric average diameter ( $d_{av}$ ), which was determined by dividing the volume flow rate of the dispersed phase to the droplet generation frequency,

$$d_{av} = \sqrt[3]{6Q_D/\pi f} \quad (1)$$

where  $Q_D$  is the volume flow rate of dispersed phase and  $f$  is the droplet generation frequency counted from the videos. The distribution of droplet diameters was analyzed from the apparent droplet diameters gauged directly from the pictures in the measurement channel. The distribution of the apparent droplet diameters represents the uniformity of the prepared emulsion and it is characterized by the polydispersity index, which is defined by the following equation:

$$\sigma = \delta^*/d_{av}^* \times 100\% \quad (2)$$

where  $\delta^*$  is the standard deviation of the apparent droplet diameter and  $d_{av}^*$  is the apparent average diameter of the droplets, an arithmetic average value of the apparent droplet diameters that was statistically analyzed from at least 200 droplets using custom-made image analysis software. According to the previous studies, monodispersed emulsion is defined when the polydispersity index is less than 5% (Xu et al. 2006).

## 3 Results and discussion

### 3.1 Droplet generation in single-pore microdevices

Since the generation rules of single droplet are still the basic laws of micro-sieve dispersion process, we give a simple discussion on the droplet generation in single-pore

microdevices at the beginning of this paper. In our previous works, the droplet generation process from a micrometer screen pore was studied. It was found that the droplet size was mainly determined by the shearing force of continuous phase and the interfacial tension (Xu et al. 2005). Some other researchers did similar works in their investigations too (van der Graaf et al. 2004). However, almost all of those works focused on the droplet generation in free shearing space (channel width much larger than the droplet size), which is far from many actual micro-sieve dispersion process in operation. Thus, we gave a study on the droplet generation process in the relatively confined shearing space and tested the effect of channel structure on the droplet size.

In the experiment, it was found that the droplets ruptured regularly in microdevices D<sub>1</sub>, D<sub>2</sub>, and D<sub>3</sub> just as they did in common T-junction microfluidic devices (Xu et al. 2006; Wang et al. 2009b). Actually, D<sub>1</sub>, D<sub>2</sub>, and D<sub>3</sub> have so similar structures that they can be seemed as big T-junction microfluidic devices. The generated droplets are monodispersed with polydispersity index less than 3% and their average diameters are given in Fig. 2. From the figure, it can be seen that the Ca number of continuous phase ( $Ca_C = \mu_C u_C / \gamma$ ) affects the droplet size very much. The droplet diameter changes from 0.3 to 1.3 mm with the variation of  $Ca_C$  ranging from 0.03 to 0.0003. The enlargement of channel width induces the droplet enlargement. Different from the droplet generation in free shearing space, where the flow of dispersed phase has little effect on the shearing speed of continuous phase, the droplet generation in confined shearing space is much more complicated. The shearing force acting on the droplet increases with the droplet growth due to the narrowing of gutters between droplet surface and channel walls. To overcome the interfacial tension and pinch off, the droplet need to grow bigger in the wider channel to get enough shearing force. We found the hydraulic diameter of the main channel ( $d_e = 2wh/(w+h)$ ) could be adopted to unite the scaling laws in those microdevices by defining a dimensionless average droplet diameter ( $d_{av}/d_e$ ). The dimensionless average droplet diameter has a linear relation with  $Ca_C^{-1/4}$  as shown in Fig. 2, which is very close to our previous conclusions in T-junction microchannels (Wang et al. 2009b; Xu et al. 2006). From the experimental results, we can get the following equation:

$$d_{av}/d_e = 0.22Ca_C^{-1/4}. \quad (3)$$

### 3.2 Dispersion rules in the microdevices with independent radial-array pores

In the micro-sieve dispersion devices, there are two methods to control the feeding of dispersed phase. One is fixing the incoming flow rate of dispersed phase in each pore and the

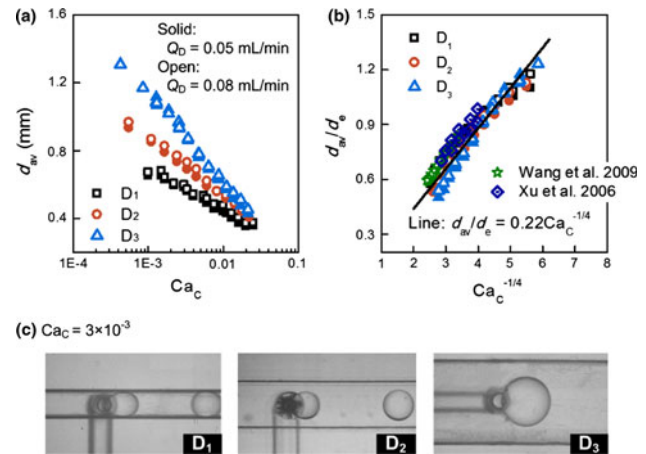


**Fig. 2** **a** The variation of average droplet diameters according to the Ca number of continuous phase in D<sub>1</sub>, D<sub>2</sub>, and D<sub>3</sub>. **b** The variation of dimensionless average droplet diameters according to the  $Ca_C^{-1/4}$  comparing with the results in our previous works (the work of Wang et al. (2009a, b) used T-junction microchannel that has a isosceles trapezoid cross section with 0.26 mm in short edge, 0.45 mm in long edge and 0.32 mm in depth. The work of Xu et al. (2006) used T-junction microchannel that has a rectangle cross section with 0.3 mm width and 0.2 mm in depth.). **c** Pictures of the generating droplets in D<sub>1</sub>, D<sub>2</sub>, and D<sub>3</sub>

other is fixing the inlet pressure of each pore. In this section, we discuss the first situation. Using individual inlet channels with individual pumps, the flow rates in micro-sieve pores of devices D<sub>4</sub> and D<sub>5</sub> can be controlled equally. The experimental results are plotted in Fig. 3. The left side of this picture gives the droplet generation process and it can be seen the droplets are rupturing alternately, the same as our previous observation (Wang et al. 2009a). The repulsion between growing droplets, owing to the steric confinement, makes the droplets generate regularly, which costs the lowest potential energy. All droplets prepared in this experiment were monodispersed with polydispersity indexes less than 4%. Figure 3c shows the variation of the average droplet diameter with the adjustments of  $Ca_C$  and channel structure. It can be seen the scaling laws in D<sub>4</sub> and D<sub>5</sub> are very close to those in D<sub>1</sub>. Different from the results in D<sub>2</sub> and D<sub>3</sub>, the droplet sizes in D<sub>4</sub> and D<sub>5</sub> hardly change with the enlargement of channel width. The reason for this phenomenon is that the steric confinement between droplets not only affects the droplet generation period but also the shearing effect from continuous phase, which makes the channel hydraulic diameter for droplet generation in D<sub>4</sub> and D<sub>5</sub> like D<sub>1</sub>, but unlike D<sub>2</sub> and D<sub>3</sub>.

### 3.3 Dispersion rules in the microdevices with independent axial-array pores

Besides the radial-array pores, there are axial-array pores in micro-sieve dispersion devices too. To investigate the

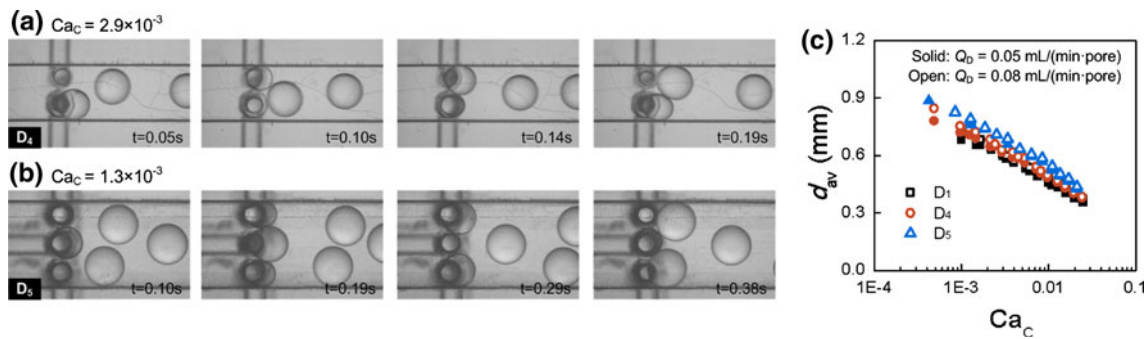


**Fig. 3** **a, b** The recorded pictures of droplet generation processes in  $D_4$  and  $D_5$ . **c** The average droplet diameters according to the Ca number in  $D_4$ ,  $D_5$ , and  $D_1$ .  $ml/(min\ pore)$  milliliter per minute for one pore

effect of axially arranged pores on the droplet generation process, microdevices  $D_6$  and  $D_7$  were made. A new phenomenon occurring in the axial-array devices is the formation of satellite droplets as shown in Fig. 4a. These small droplets are pinched off by the cutting from upstream droplets, which affect the uniformity of prepared emulsions. However, by adjusting experimental conditions, it is found that the satellite droplet disappears at low phase ratio of the two phases ( $Q_D/Q_C$ ) and regular generation comes back with monodispersed droplets, as shown in Fig. 4b. The reason for this phenomenon can be explained by Fig. 4c. The incoming of dispersed phase fluid from the upstream pore increases the shearing speed above the downstream pore. Thus, microdroplets with different sizes are prepared on those pores with different generation periods, as shown in Fig. 4d and e. Inconsistent generation periods cause collisions between flowing droplets and growing droplets, which produce satellite droplets. To make the satellite droplets disappear, low dispersed phase ratio is important to weaken the collision effect.

We measured the distribution of droplet sizes in the experiment, as shown in Fig. 5a and b. The prepared droplets become uniform at phase ratios lower than 1/6 and the reason about this can be explained from the generation periods in Fig. 4. The average droplet diameters in  $D_6$  and  $D_7$  are given in Fig. 5c comparing with the droplet sizes in  $D_2$ . This figure shows the scaling law in independent axial-array-pore dispersion devices is the same as that in single-pore dispersion devices. From Figs. 4 and 5, we can also find the generation rules in  $D_6$  and  $D_7$  are almost the same. Since the axial distances in  $D_6$  and  $D_7$  are larger than any of the generated droplets, the interaction between two growing droplets does not exist in both devices. Thus, the distance between micro-sieve pores does not affect the droplet generating period, which makes little effect on the droplet size and distribution in the present work.

### 3.4 Dispersion rules in the microdevices with connected radial-array pores

The microdevices with independent micro-sieve pores are effective tools for the preparation of monodispersed emulsions. However, their operations are complicated. The more commonly used micro-sieve dispersion devices are the connected array-pore devices, which have inlet chambers of dispersed phase. Unlike the independent array-pore device, the connected array-pore device provides equal trans-pore pressure beside the micro-sieve plate. Due to this simplified structure, the flow distribution of dispersed phase fluids among pores becomes a new problem. In the experiment, we did our best to make the shapes of the micro-sieve pores consistent, but the flows were still inequality. The experimental results in a connected radial-array-pore device are given in Fig. 6. At low flow rate of dispersed phase, there is no droplet generating in some pores, which can be seemed as inactive pores (Abrahamse et al. 2002). The active pores appeared randomly at the beginning of the experiment and some of them had high possibility to be activated. This may be caused by the tiny differences of pore structures. The number of active pores increases with the increasing of dispersed phase feeding rate due to the enlargement of trans-pore pressure, which is in accord with the results from Abrahamse' group (Gijbetsen-Abrahamse et al. 2003). Except for the pore activity, the flow resistances in and above micro-sieve pores affect the flow distribution too. According to the force analysis on the dispersed phase fluid (Li et al. 2009c), the resistance mainly comes from two sources: the resistance from pore wall and the Young–Laplace pressure from the droplet surface. We can use a schematic graph, Fig. 6b, to show these resistances. Since the Young–Laplace pressure is determined by the droplet radius ( $r$  in Fig. 6), which changes with the droplet growth, the flow rates of dispersed phase in pores are not stable (Wang et al. 2009a). Additionally, at low Ca numbers of continuous phase the droplets grow big and the steric hindrance between droplets

**Fig. 4** **a, b** The recorded pictures of droplet generation processes in  $D_6$  and  $D_7$ . The satellite droplets are formed by the cutting from upstream droplets. **c** The schematic diagram of shearing flow rates on the upstream pore and downstream pore. **d, e** The droplet generation periods in  $D_6$  and  $D_7$

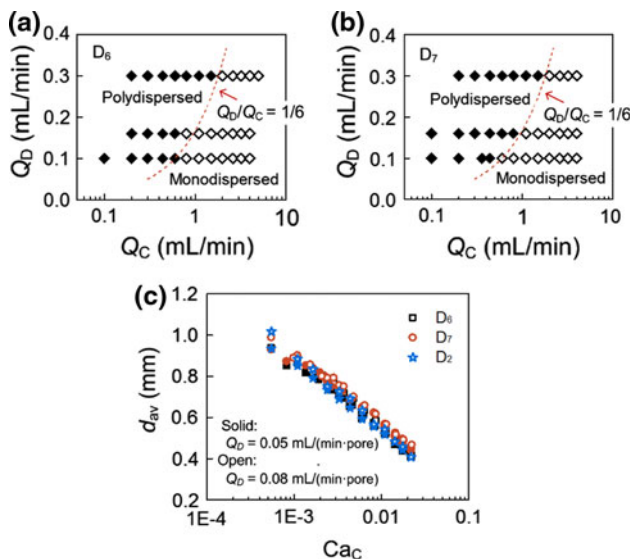
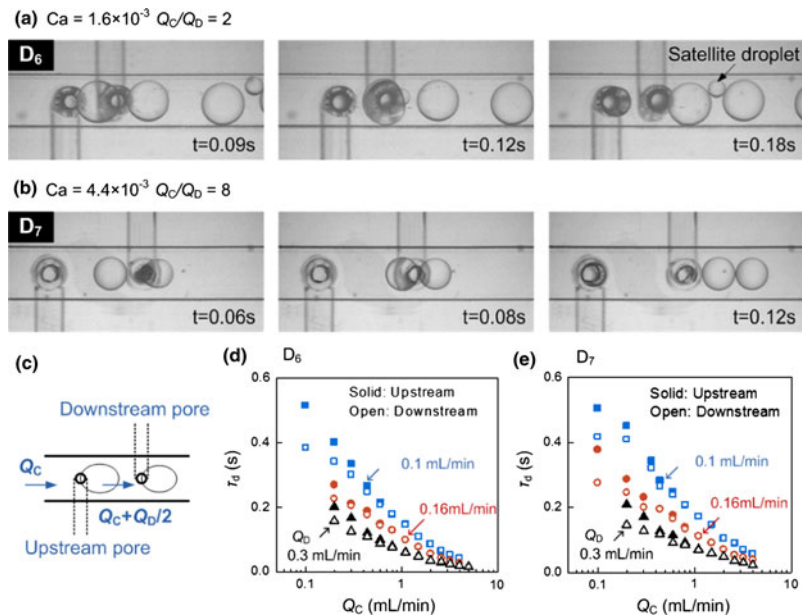


**Fig. 5** **a, b** The effect of phase ratio on the distribution of the droplet sizes in  $D_6$  and  $D_7$ . In this work, the monodispersed droplets are defined as the droplets whose polydispersity index is less than 5% (Xu et al. 2006). **c** The average droplet diameters in  $D_6$  and  $D_7$  with the comparison of those in  $D_2$

strongly affects their shapes. This causes serious direction fluctuation of the shearing fluid above pores and leads to polydispersed droplet generation as shown in Figs. 6a and 7a. At high  $Ca$  numbers, the sizes of droplet become small and uniform during their growth, owing to the weak resistance disturbances above pores. At  $Ca$  numbers larger than 0.01 the droplet sizes are less than 0.6 mm, which are smaller than the center distance between pores. Thus, the steric hindrances among growing droplets are weak enough to bring uniform droplet sizes. The average droplet diameters

with the variation of  $Ca$  numbers are given in Fig. 7b. It shows the droplet size decreases with the increase of  $Ca_C$  and decreases with the increase of active pore numbers. The increase of active pore numbers enhances the steric confinement between growing droplets, which reduces the droplet sizes (Abrahamse et al. 2002). The  $Ca$  number larger than 0.01 is the key factor for the preparation of monodispersed emulsions in this work.

### 3.5 Dispersion rules in the microdevices with connected axial-array pores

As the last situation, we discuss the droplet generation in connected axial-array-pore device  $D_9$  in this section. In the experiment, it was observed that the collision between growing droplets and flowing droplets still existed. Due to the effect of the satellite droplets and the flow distribution between micro-sieve pores, most of the formed droplets are polydispersed. Monodispersed droplets can only be prepared at  $Ca_C$  larger than 0.01 and phase ratio lower than 1/6. The experimental results are given in Fig. 8. These results are in accord with the above discussions. Thus, the conclusion is that high  $Ca$  number and low phase ratio are necessary for the preparation of monodispersed emulsion in micro-sieve dispersion device. The average droplet diameters in  $D_9$  are given in Fig. 8b. It can be seen that the scaling laws are coincident at different active pore numbers.

### 3.6 Test of droplet generation rules with common micro-sieve dispersion devices

In the last section, we give a discussion on the droplet generation rules in common micro-sieve dispersion devices.

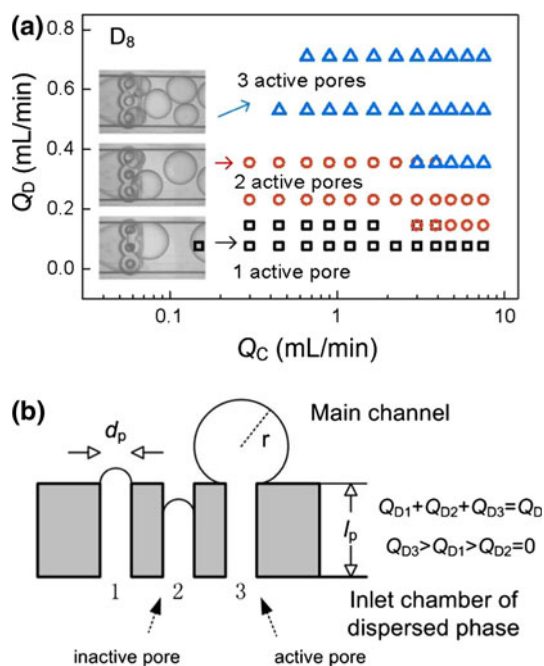


**Fig. 6** **a** The active pores at different operating conditions. **b** The schematic diagram of dispersed phase flow distribution in a connected-pore microdevice

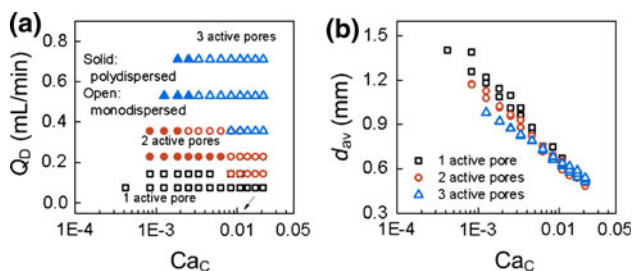


**Fig. 7** **a** The droplet distributions at different operating conditions in  $D_8$ . **b** The average droplet diameters according to the  $Ca$  number.  $Q_D = 0.05\text{--}0.71$  ml/min

Two connected array-pore microdevices,  $D_{10}$  and  $D_{11}$ , with  $2 \times 2$  and  $3 \times 3$  micro-sieve pores were developed to test the scaling law and the distribution of formed droplets. The average droplet diameters in those microdevices are shown in Fig. 9, which indicates that the droplet size is mainly determined by the  $Ca$  number of continuous phase too. The average droplet diameters are in accord with the linear relation with  $Ca_C^{-1/4}$ . Comparing with Eq. 3, it is found the effective hydraulic diameter of devices  $D_{10}$  and  $D_{11}$  is about 0.8 mm, which is very close to the hydraulic diameter of  $D_1$ . The flow rates of dispersed phase are controlled from 0.6 to 2.4 ml/min in the experiment to make the active pores larger than 3 in  $D_{10}$  and larger than 7 in  $D_{11}$ . In these conditions, the running capacity of dispersed phase in  $D_{11}$  is about 30 times higher than that in  $D_3$ . From Fig. 9, it can be seen the growing droplets on the upstream pores generate regularly, the same

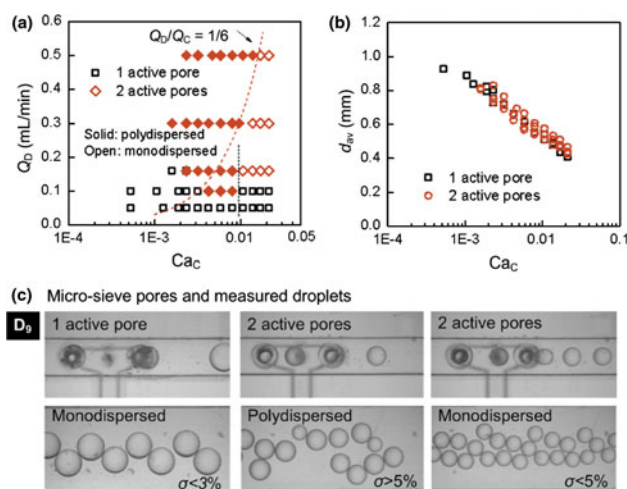


**Fig. 8** **a** The droplet distributions at different operating conditions in  $D_9$ . **b** The average droplet diameters according to the  $Ca$  number.  $Q_D = 0.05\text{--}0.5$  ml/min. **c** The recorded pictures of micro-sieve pores in  $D_9$  and the formed droplets in the measurement channel

as those in devices  $D_4$ ,  $D_5$ , and  $D_8$ , but irregularly on the downstream pores. Harsh collisions between flowing droplets and growing droplets affect the droplet generation process above the downstream pores and most of the generated droplets are polydispersed. The polydispersity indexes at different experimental conditions are given in Fig. 10, which are ranging from 4 to 21%. Partition lines in Fig. 10 are used to separate the polydispersed droplets and the monodispersed droplets. It is found that monodispersed droplets can be only prepared at  $Ca_C$  larger than 0.01 and phase ratio lower than 1/6, which is the same as the above conclusions.

### 4 Conclusion

This work presents the droplet generation rules in micro-sieve dispersion devices for the emulsions. To give a clear display of the generation process, nine kinds of microdevices labeled from  $D_1$  to  $D_9$  are designed with single pore, radial pores, and axial pores. According to the average droplet diameters, it is found the channel size and  $Ca$  number of continuous phase affect the droplet size significantly. The dimensionless average droplet diameter ( $d_{av}/d_c$ ) can be represented by a linear relation with  $Ca_C^{-1/4}$  in both the single-pore and multi-pore micro-sieve devices. The steric confinement between growing droplets on radial pores affects the effective hydraulic diameter of the main channel. The collision between flowing droplets and growing droplets produces satellite droplets, which affects the emulsion uniformity. Two feeding methods of dispersed phase are applied in this work using independent pores and connected pores, respectively. It is found that monodispersed droplets are easy to produce in the

**Fig. 9** **a** The average droplet diameters according to the Ca number in  $D_{10}$  and  $D_{11}$ .  $Q_D = 0.6\text{--}2.4$  ml/min. **b, c** The recorded pictures of droplet generation processes in  $D_{10}$  and  $D_{11}$  with the flowing droplets in their measurement channels

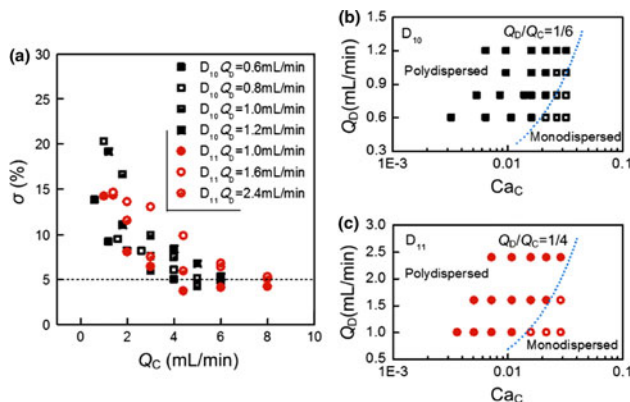
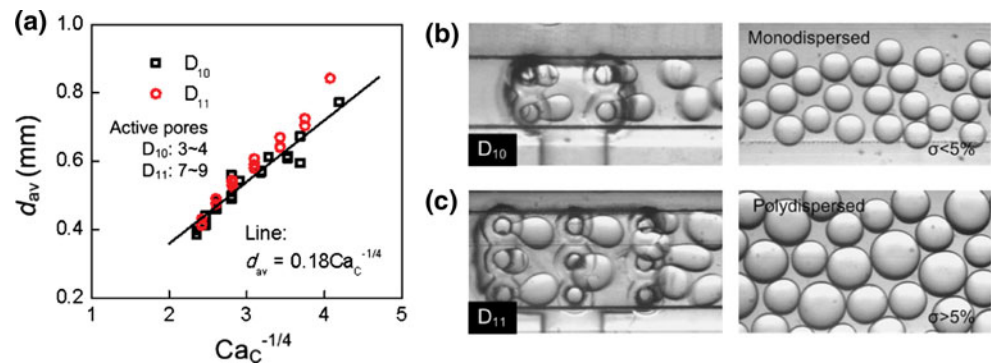


**Fig. 10** **a** The variation of polydispersity indexes at different operating conditions in  $D_{10}$  and  $D_{11}$ . **b, c** The droplet distributions

independent-pore devices but hard to produce in the connected-pore devices, due to the unstable flow rates of dispersed phase in the pores and the strong steric hindrance between droplets. By testing the generation rules with commonly used micro-sieve dispersion devices, which have  $2 \times 2$  and  $3 \times 3$  micro-sieve pore arrays, it is found that the scaling law in the single-pore devices is still available in the multi-pore devices and monodispersed droplets can be prepared at  $Ca_C$  higher than 0.01 and phase ratio ( $Q_D/Q_C$ ) lower than 1/6 in the present experiments.

**Acknowledgments** We gratefully acknowledge the supports of the National Natural Science Foundation of China (21036002, 20876084) and SRFDP (20090002110070) for this work.

## References

- Abrahamse AJ, van Lierop R, van der Smana RGM, van der Padt A, Booma RM (2002) Analysis of droplet formation and interactions during cross-flow membrane emulsification. *J Membr Sci* 204:125–137
- Choi J, Lee SK, Lim JM, Yang SM, Yi GR (2010) Designed pneumatic valve actuators for controlled droplet breakup and generation. *Lab chip* 10:456–461
- Christopher GF, Noharuddin NN, Taylor JA, Anna SL (2008) Experimental observations of the squeezing-to-dripping transition in T-shaped microfluidic junctions. *Phys Rev E* 78:036317
- Cubaud T, Mason TG (2008) Capillary threads and viscous droplets in square microchannels. *Phys Fluid* 20:053302
- de Menech M, Garstecki P, Jousse F, Stone HA (2008) Transition from squeezing to dripping in a microfluidic T-shaped junction. *J Fluid Mech* 595:141–161
- Engl W, Backov R, Panizza P (2008) Controlled production of emulsions and particles by milli- and microfluidic techniques. *Curr Opin Colloid Interface Sci* 13:206–216
- Felbel J, Reichert A, Kielpinski K, Urban M, Henkel T, Hafner N, Durst M, Weber J (2008) Reverse transcription-polymerase chain reaction (RT-PCR) in flow-through micro-reactors: thermal and fluidic concepts. *Chem Eng J* 135S:S298–S302
- Geerken MJ, Lammertink RGH, Wessling M (2007) Interfacial aspects of water drop formation at micro-engineered orifices. *J Colloid Interface Sci* 312:460–469
- Geerken MJ, Groenendijk MNW, Lammertink RGH, Wessling M (2008) Micro-fabricated metal nozzle plates used for water-in-oil and oil-in-water emulsification. *J Membr Sci* 310:374–383
- Gijsbertsen-Abrahamse AJ, van der Padt A, Booma RM (2003) Status of cross-flow membrane emulsification and outlook for industrial application. *J Membr Sci* 217:141–150
- Gijsbertsen-Abrahamse AJ, van der Padt A, Booma RM (2004) Status of cross-flow membrane emulsification and outlook for industrial application. *J Membr Sci* 230:149–159
- Guillot P, Colin A, Utada AS, Ajdari A (2007) Stability of a jet in confined pressure-driven biphasic flows at low Reynolds numbers. *Phys Rev Lett* 99:104502
- Kjeang E, Djilali N, Sinton D (2009) Microfluidic fuel cells: a review. *J Power Sources* 186:353–369
- Kobayashi I, Takano T, Maeda R, Wada Y, Uemura K, Nakajima M (2008) Straight-through microchannel devices for generating monodisperse emulsion droplets several microns in size. *Microfluid Nanofluid* 4:167–177
- Lao KL, Wang JH, Lee GB (2009) A microfluidic platform for formation of double-emulsion droplets. *Microfluid Nanofluid* 7:709–719
- Li SW, Xu JH, Wang YJ, Luo GS (2009a) Liquid-liquid two-phase flow in pore array microstructured devices for scaling-up of nanoparticle preparation. *AIChE J* 55:3041–3051
- Li SW, Xu JH, Wang YJ, Lu YC, Luo GS (2009b) Low-temperature bonding of poly-(methyl methacrylate) microfluidic devices under an ultrasonic field. *Micromech Microeng* 19:015035
- Li SW, Xu JH, Wang YJ, Luo GS (2009c) A new interfacial tension measurement method through a pore array micro-structured device. *J Colloid Interface Sci* 331:127–131
- Marmottant P, Raven JP (2009) Microfluidics with foams. *Soft Matter* 5:3385–3388



- Nie ZH, Seo MS, Xu SQ, Lewis PC, Mok M, Kumacheva E, Whitesides GM, Garstecki P, Stone HA (2008) Emulsification in a microfluidic flow-focusing device: effect of the viscosities of the liquids. *Microfluid Nanofluid* 5:585–594
- Nisisako T, Torii T (2008) Microfluidic large-scale integration on a chip for mass production of monodisperse droplets and particles. *Lab Chip* 8:287–293
- Panic S, Loebbecke S, Tuercke T, Antes J, Boskovi D (2004) Experimental approaches to a better understanding of mixing performance of microfluidic devices. *Chem Eng J* 101: 409–419
- Park JI, Nie ZH, Kumachev A, Abdelrahman AI, Binks BP, Stone HA, Kumacheva E (2009) A microfluidic approach to chemically driven assembly of colloidal particles at gas–liquid interfaces. *Angew Chem Int Ed* 48:5300–5304
- Razzaq T, Glasnov TN, Kappe CO (2009) Accessing novel process windows in a high-temperature/pressure capillary flow reactor. *Chem Eng Technol* 32:1702–1716
- Sevonkaev I, Matijevic E (2009) Formation of magnesium fluoride particles of different morphologies. *Langmuir* 25:10534–10539
- Steggmans MLJ, Schroen KGPH, Boom RM (2009) Characterization of emulsification at flat microchannel Y-junctions. *Langmuir* 25:3396–3401
- Teh SY, Lin R, Hung LH, Lee AP (2008) Droplet microfluidics. *Lab chip* 8:98–220
- van der Graaf S, Schroën CGPH, van der Sman RGM, Boom RM (2004) Influence of dynamic interfacial tension on droplet formation during membrane emulsification. *J Colloid Interface Sci* 277:456–463
- van Steijn V, Kleijn CR, Kreutzer MT (2009) Flows around confined bubbles and their importance in triggering pinch-off. *Phys Rev Lett* 103:214501
- Wang K, Lu YC, Xu JH, Tan J, Luo GS (2009a) Liquid-liquid microdispersion in a double-pore T-shaped microfluidic device. *Microfluid Nanofluid* 6:557–564
- Wang K, Lu YC, Xu JH, Luo GS (2009b) Determination of dynamic interfacial tension and its effect on droplet formation in the T-shaped microdispersion process. *Langmuir* 25:2153–2158
- Xu JH, Luo GS, Chen GG, Wang JD (2005) Experimental and theoretical approaches on droplet formation from a micrometer screen hole. *J Membr Sci* 266:121–131
- Xu JH, Li SW, Tan J, Wang YJ, Luo GS (2006) Preparation of highly monodisperse droplet in a T-junction microfluidic device. *AIChE J* 52:3005–3010
- Xu JH, Tan J, Li SW, Luo GS (2008a) Enhancement of mass transfer performance of liquid–liquid system by droplet flow in microchannels. *Chem Eng J* 141:242–249
- Xu JH, Li SW, Tan J, Luo GS (2008b) Correlations of droplet formation in T-junction microfluidic devices: from squeezing to dripping. *Microfluid Nanofluid* 5:711–717